THE PHOTOGRAMMETRIC RECORD

The Photogrammetric Record 26(134): 190–211 (June 2011)
DOI: 10.1111/j.1477-9730.2011.00641.x

PHOTOGRAMMETRIC PROCESSING OF LOW-ALTITUDE IMAGES ACQUIRED BY UNPILOTED AERIAL VEHICLES

YONGJUN ZHANG (zhangyj@whu.edu.cn)
JINXIN XIONG (einbetter1995@hotmail.com)
LIJUAN HAO (lijuan_hao@sina.cn)
School of Remote Sensing and Information Engineering, Wuhan University, China

Abstract

Low-altitude images acquired by unpiloted aerial vehicles have the advantages of high overlap, multiple viewing angles and very high ground resolution. These kinds of images can be used in various applications that need high accuracy or fine texture. A novel approach is proposed for parallel processing of low-altitude images acquired by unpiloted aerial vehicles, which can automatically fly according to predefined flight routes under the control of an autopilot system. The general overlap and relative rotation angles between two adjacent images are estimated by overall matching with an improved scale-invariant feature transform (SIFT) operator. Precise conjugate points and relative orientation parameters are determined by a pyramid-based least squares image matching strategy and the relative orientation process. Bundle adjustment is performed with automatically matched conjugate points and interactively measured ground control points. After this aerial triangulation process the high-resolution images can be used to advantage in obtaining precise spatial information products such as digital surface models, digital orthophotomaps and 3D city models. A parallel processing strategy is introduced in this paper to improve the computational time of the photogrammetric process. Experimental results show that the proposed approaches are effective for processing low-altitude images, and have high potential for the acquisition of spatial information at large mapping scales, with rapid response and precise modelling in three dimensions.

KEYWORDS: 3D city model, accuracy analysis, bundle block adjustment, image matching, large scale urban mapping, unpiloted aerial vehicle

INTRODUCTION

IMAGE ACQUISITION is one of the most expensive steps in photogrammetric applications. The development of flexible and efficient techniques to obtain high-resolution images has been the primary purpose of many photogrammetric researchers and practitioners. As compared with film-based cameras, digital cameras are advantageous in obtaining images with large overlap (such as 80% forward overlap) without increasing the number of strips. In this case, every ground feature usually appears in at least five corresponding images. High overlap image

sequences are also advantageous for image matching and 3D reconstruction (Zhang et al., 2005).

Along with the development of unpiloted aerial vehicles (UAVs), popularisation of non-metric digital cameras and other progress in photogrammetric technologies, low-altitude images have been a subject of considerable interest in the photogrammetric community. The most used low-altitude platforms for image data acquisition are helicopters (Zhang et al., 2005), remotely controlled model aircraft (Nogami et al., 2002; Coppa et al., 2010) or tethered balloons (Huang and Lin, 2003; Altan et al., 2004). One of the major advantages of UAVs is that they can conveniently acquire images of very high ground resolution under cloud. Low-altitude high-resolution images have great potential in many applications such as large scale mapping, true orthophoto generation, archaeology and 3D city modelling, especially where a quick response is required, as in disaster monitoring.

Many projects involving photogrammetric processing of low-altitude images have been reported (including Karras et al., 1999; Altan et al., 2004; Bitelli et al., 2004; Zhang et al., 2005; Lin, 2008; Nagai et al., 2008). For example, 0·04 m height accuracy has been achieved with high-resolution images acquired from a tethered balloon (Altan et al., 2004). However, data acquisition by unpiloted platforms and especially efficient processing of low-altitude images are still at an early stage (Zhang, 2008).

The typical characteristic of images acquired from low-altitude platforms is that no predefined relationship between adjacent images can be strictly guaranteed. There are usually large overlap variations and large rotation angles between adjacent images, and very large parallax discontinuities of features above the ground such as high buildings. Thus the terrain continuity constraint that is used by most traditional matching algorithms is invalid, and most traditional photogrammetric software cannot deal with low-altitude images.

This paper is an extended and improved version of Zhang (2008), thanks to the inclusion of investigations of a parallel processing strategy and of overall matching with a scale-invariant feature transform (SIFT) operator. Textured 3D building model generation of the test area is also discussed. As compared with the approaches in the literature, this proposed approach can find enough conjugate points among adjacent low-altitude images fully automatically, thereby overcoming the biggest difficulty of processing low-altitude images efficiently. Moreover, high-precision bundle adjustment with additional parameters is also contributed in this approach. The general strategy for photogrammetric processing of low-altitude images, the basic concept of parallel processing, the composition of the low-altitude photogrammetric system developed here and the data acquisition for these experiments are described in the next section. Afterwards, detailed approaches of photogrammetric processing, including parallel processing strategy, overall and precise image matching, relative orientation and model link, bundle adjustment, digital surface model (DSM) and digital orthophotomap (DOM) generation, and 3D building model visualisation are discussed. The experimental results of photogrammetric processing and the generation of digital photogrammetric products are then addressed. Finally, conclusions are drawn and appropriate further work is highlighted.

General Strategy and Data Sources

General Strategy

The photogrammetric processing of low-altitude images, including image matching, relative orientation, bundle adjustment, DSM and DOM generation, and 3D building reconstruction are the content of the current work. The imagery used for the experiments was automatically acquired by a low-altitude photogrammetric system based on an unmanned

airship. Automatic estimation of approximate overlap and rotation angles between adjacent images is one of the most difficult problems in processing low-altitude images. Firstly, the overlap and relative rotation angle between adjacent images are estimated by conjugate points matched using an improved SIFT algorithm. Then precise conjugate points are acquired by least squares matching (LSM) within a local search range. The image matching process is constrained by epipolar lines, which are determined by relative orientation parameters. The matched image points and measured ground control points (GCPs) are used for bundle block adjustment with collinearity equations. Digital ortho-images can be rectified after a DSM is generated by dense image matching and forward intersection. All time-consuming processes are realised by multi-core and multi-computer parallel processing strategies. Finally, the aerial triangulated images are also used for large scale mapping and 3D building model generation.

Scheme of Parallel Processing

There are many time-consuming processes, such as image matching, DSM and DOM generation, which determine the computational time of photogrammetric processing (Zhang et al., 2009). A parallel processing strategy based on multi-core and multi-computer systems is used in this paper to improve the computational time. As shown in Fig. 1, multi-core computers are used as computing nodes, which are connected to a high-performance disk array by a gigabyte switch. There is also a workstation for the operator to define and monitor all parallel processing tasks, such as image matching, DSM and DOM generation.

The general procedure of parallel processing is that a task list is firstly built and then assigned to available computing nodes to perform the corresponding processing. As long as tasks to be performed are defined via the workstation, the task dispatch software can automatically dispatch all tasks to the available computing nodes and monitor the current status of all nodes. All software modules on the computing nodes are specially programmed to take

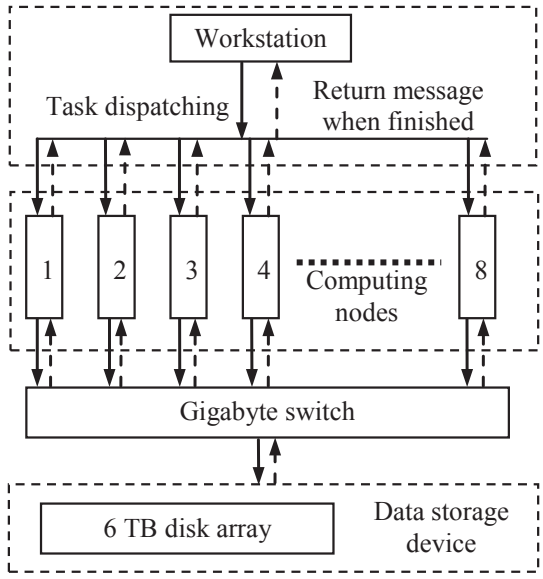

FIG. 1. General scheme of parallel processing.

full advantage of multi-core CPUs. Each node will send a message back to the workstation when the task received is finished and the node is ready to receive a new task. As a result, a parallel processing strategy is more time efficient when compared with the traditional single computer and image-by-image processing strategy.

Low-Altitude Photogrammetric System with an Airship

After several years' research in cooperation with another group, a low-altitude photogrammetric system based on an unpiloted airship has been successfully developed. The airship can automatically fly along predefined flight paths under the control of an autopilot system. The hardware of the photogrammetric system is composed of airship, autopilot system, task payload, wireless communication equipment, ground-based monitoring computer and optional global positioning system (GPS) reference station, as shown in Fig. 2.

The autopilot system is composed of a single-chip computer, GPS receiver, micro-electro-mechanical systems (MEMS) gyroscope, barometric altimeter, airspeed indicator and flying control software. The autopilot system collects real-time information such as position and speed of the unpiloted airship and automatically controls the airship in accordance with the predefined flight path. The task payload consists of a digital camera, a video camera and a three-axis stabilised platform on which the two cameras are fixed. The platform can automatically maintain predefined camera orientation against the swing or oscillation of the airship. The dashed arrows in Fig. 2 indicate control signals and information transferred from the monitoring computer on the ground to the autopilot system by wireless communication equipment, while solid arrows indicate the flying status information and data (such as real-time video) transferred from the autopilot system and task payload to the ground monitoring computer.

The technical parameters of the low-altitude photogrammetric system are as follows: length of the airship is 13·2 m, cruising speed is 30 to 40 km/h, maximum payload capacity is 15 kg, accuracy of flying track against predefined route is around 10 m, accuracy of the three-axis

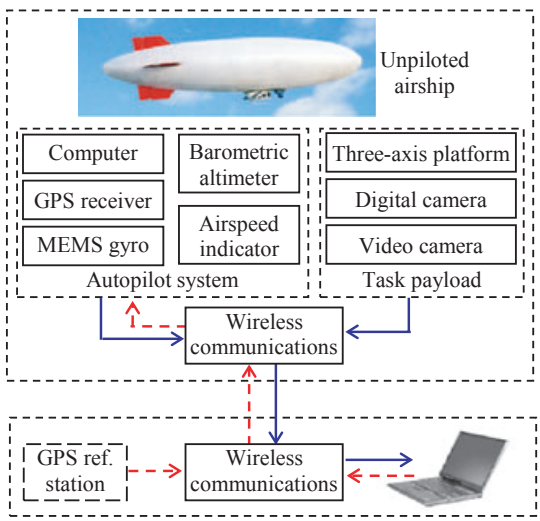

FIG. 2. Hardware of the low-altitude photogrammetric system.

stabilised platform in maintaining camera attitude is about 3 degrees in roll and pitch and 5 degrees in yaw. The non-metric still camera fixed on the platform is a Kodak Pro SLR with 3000 × 4500 pixels image format and 8 μm physical pixel size. The physical image sensor size of the camera is 24 mm × 36 mm.

Data Sources

As described above, the unpiloted airship can fly automatically in accordance with its predefined flight path. A digital camera is fixed on the three-axis stabilised platform, which can keep the camera orientation more stable than the airship itself while flying. Two sets of low-altitude images were acquired by the system. The first image data-set was acquired at a testfield in northern China (North) and the second in southern China (South).

Experimental Data of the Northern Testfield. Low-altitude images of the northern testfield, covering about 700 m × 700 m, were taken with the photogrammetric system developed for this project, using a camera with a 24 mm lens in November 2007. The flying height of the airship was about 150 m above ground, and thus the ground sampling distance (GSD) is 0·05 m. The base-to-height ratio with 60% forward overlap is 0·40. The predefined distance between two exposure stations within one strip was 28 m, and the distance between adjacent strips was 50 m, such that the forward overlap (endlap) and sidelap are 80 and 75%, respectively. A total of 299 images in 13 strips were taken with the unpiloted airship. Wind speed was about 7 m/s during image data acquisition. Fig. 3 shows the planimetric position of exposure stations of all images. As can be seen, the flight paths are nearly straight lines. The maximum planar bias between exposure point and predefined flying strip is about 5 m. The flying height was

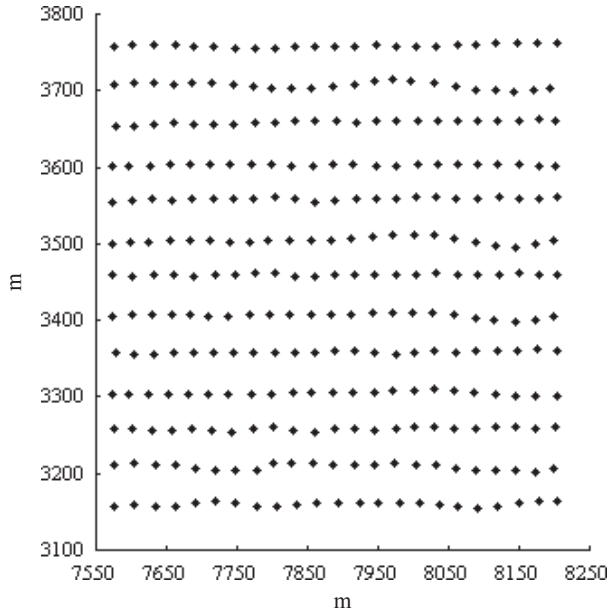

FIG. 3. Planimetric positions of photo centres of the North testfield.

FIG. 4. Stereo-images of the North testfield taken by the airship-borne system.

maintained with an accuracy of about 10 m compared with the predefined flying height. Orientation variations between adjacent images are mostly within 5 degrees, but occasionally larger than 10 degrees owing to strong and abrupt gusts of wind. Five typical stereoscopic images are shown in Fig. 4. As can be seen, the overlap and camera attitude are quite stable.

To fully evaluate the accuracy of images acquired by the low-altitude photogrammetric system, 64 funnel-shaped artificial marks were set up on the test area and measured by total station before aerial photography. The planimetric and height accuracy of these control points are all better than 0·015 m. To ensure that there is one GCP every four to six images, as required by the criteria for Chinese national mapping, all GCPs are regularly distributed in the test area, as shown in Fig. 5. The 33 points indicated by triangles are used as control points, while the other 31 points marked by squares are check points for the bundle adjustment experiments.

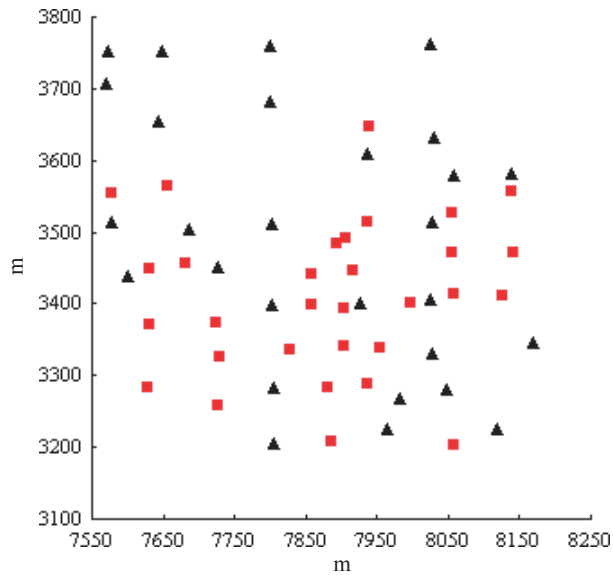

FIG. 5. Distribution of control and check points of the North testfield.

Experimental Data of the Southern Testfield. Low-altitude images of the testfield in southern China were taken in March 2008 using a 14 mm super-wide-angle lens. Ground coverage of the test area is about 8000 m × 8000 m. The flying height of the airship above ground was about 350 m, and thus the GSD is about 0·20 m. The base-to-height ratio with 60% endlap is 0·68. The predefined distance between two exposure stations within one strip was 120 m, and distance between each strip was 360 m, giving endlap and sidelap of 80 and 60%, respectively. In total 1890 images in 26 strips were taken, including four cross strips. Fig. 6 shows the planimetric position of all projection centres. Wind speed was about 7 m/s during image data acquisition. The maximum planimetric discrepancy from exposure point to predefined flying strip is about 10 m. Height accuracy when compared with predefined flying

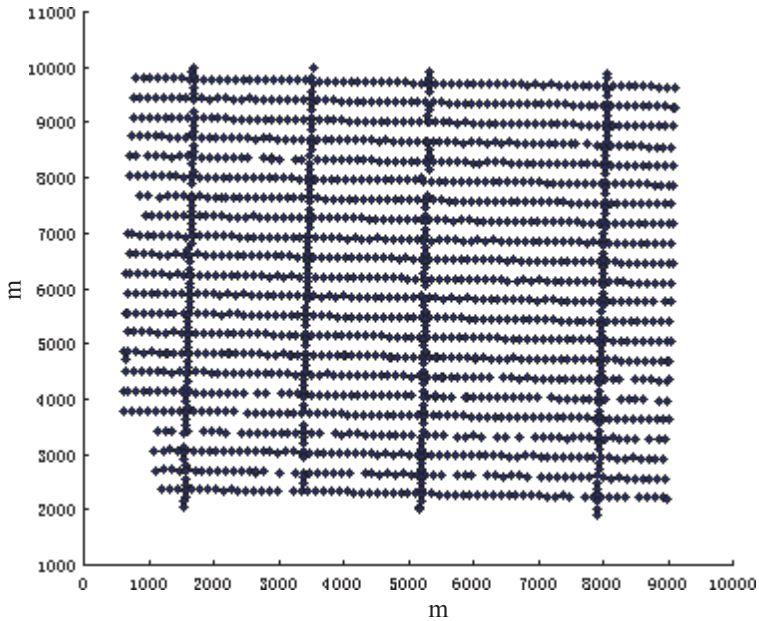

FIG. 6. Planimetric positions of photo centres of the South testfield.

FIG. 7. Stereo-images of the South testfield taken by the airship-borne system.

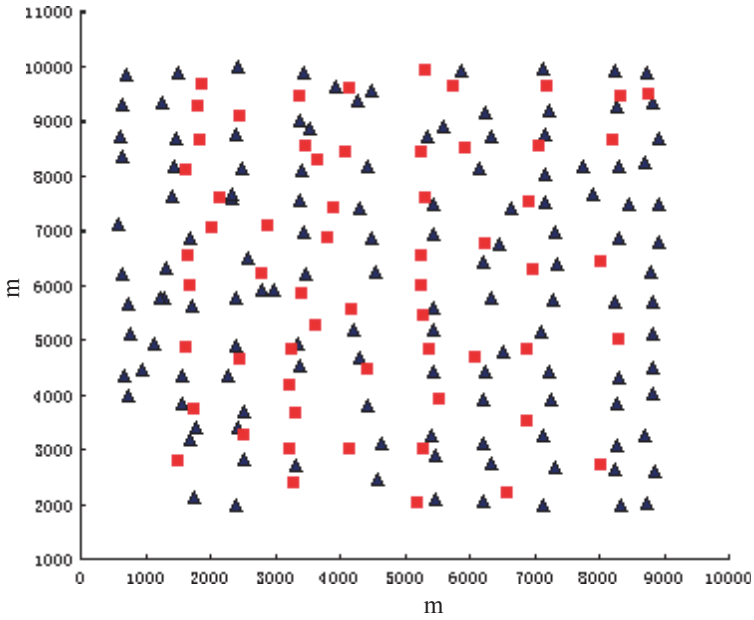

FIG. 8. Distribution of control and check points of the South testfield.

height is about 15 m, orientation variations between adjacent images are mostly within 5 degrees, rarely larger than 15 degrees resulting from gusts of wind. Five typical stereo-images are shown in Fig. 7. As can be seen, the overlap and camera attitude are stable and conformed closely to the predefined values.

To fully evaluate the accuracy of images acquired by the low-altitude photogrammetric system, a total of 190 ground features such as zebra crossing corners and sewer cover centres were measured by dual-frequency differential GPS receivers and used as control points for bundle adjustment. The planimetric and height accuracy of these control points are about 0·03 m. Fig. 8 shows the distribution of these ground control points. The 130 points indicated by triangles are used as control points, while the remaining 60 points marked by squares are check points for the bundle adjustment experiments.

PHOTOGRAMMETRIC PROCESSING OF LOW-ALTITUDE IMAGES

Characteristics of Low-Altitude Images

Camera orientations usually vary among adjacent low-altitude images because the attitude of the stabilised platform often changes when the UAV encounters strong gusts of wind. For example, 3 degrees of variation in pitch and roll angle will result in about ±5% changes in endlap and sidelap. In extreme circumstances, the real overlap between adjacent images will change about 10% compared with the predefined overlap, thus becoming 70 to 90% if the predefined endlap is 80% or 20% to 40% if the predefined sidelap is 30%. Variation in yaw angle also brings overlap problems. Furthermore, high trees and buildings cause local overlap changes. As shown in Fig. 9, the above-mentioned deficiencies distinctly worsen the problem

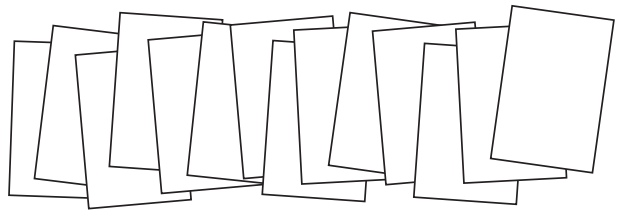

FIG. 9. Sketch map of images acquired by a UAV in extreme circumstances.

of image matching. Nearly all current digital photogrammetric workstations cannot deal with low-altitude images effectively. The key challenge in matching low-altitude images is to find some overall optimal conjugate points and thus estimate the orientation variation between image pairs.

Image Matching

Image matching is a fundamental aspect of many problems in computer vision, including object recognition, solving for 3D structure from multiple images, stereoscopic correspondence and motion tracking. It is also a prerequisite for bundle adjustment and 3D information extraction in photogrammetry. In this paper, the image matching process is divided into three steps: overall matching with a SIFT operator, feature point extraction and fine matching.

Overall Matching with SIFT Operator. The scale-invariant feature transform (SIFT) operator (Lowe, 1999, 2004) can transform image data into scale-invariant coordinates relative to local features. These features are invariant to image scaling and rotation, and partially invariant to changes in illumination and 3D camera viewpoint. This operator has good potential for matching between low-altitude image pairs that usually have large rotation angles. According to Lowe (1999, 2004), the major stages of computation used to generate a set of image features are: scale-space extrema [*sic*] detection, keypoint localisation, orientation assignment and keypoint descriptor. For image matching, SIFT features are separately extracted from each image of a stereopair and stored in a database. The two images are matched by individually comparing each feature of the second image to all features of the previous image based on Euclidean distance between feature vectors.

An important aspect of the SIFT approach is that it generates large numbers of features that densely cover the image. Matching between two feature point data-sets is thus very time-consuming. Furthermore, a global search strategy will result in many false matches, which will definitely influence subsequent processes such as object recognition.

Very large overlap and rotation angle variations, for example, 40% overlap changes and more than 30-degree rotation angles between adjacent images, are impossible for the low-altitude images discussed here, because the platform always flies forward along the predefined route. So in the overall matching process, the searching range for conjugate points in the right image for a certain feature point in the left image should be less than 40% of the image format, in order to avoid many mismatches. For example, if the predefined endlap is 70%, searching range in the right image should between 50 and 90%. As shown in Fig. 10, the black rectangle represents the left image of a stereopair and the magenta rectangle represents the right image with 70% predefined endlap. Searching range is from 50% (blue rectangle in Fig. 10(a)) to 90% (dashed red rectangle in Fig. 10(a)) in the along-strip direction, and from 80% (blue

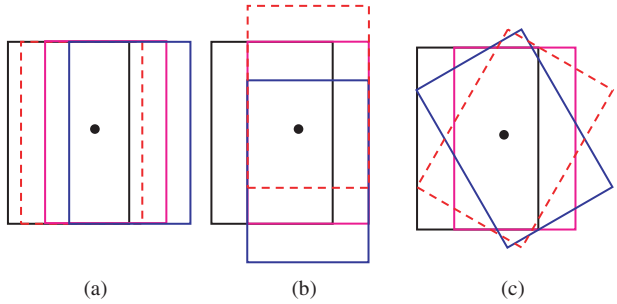

FIG. 10. Searching range for conjugate points in the right image.

rectangle in Fig. 10(b)) to 120% (dashed red rectangle in Fig. 10(b)) in the across-strip direction. Changes of yaw angle (κ) with at most ±30 degrees is also considered (blue and dashed red rectangle in Fig. 10(c)). In fact, the searching range in real images is a combination of all three cases. This strategy of predefined searching range not only improves the computational time of the SIFT operator, but also decreases the possibility of obtaining many mismatches with a global searching strategy. When SIFT features in a stereopair are compared with each other, only point pairs within the predefined searching range and also with Euclidean distance ratio higher than the predefined threshold are treated as overall conjugate points. As long as five or more conjugate points are successfully found, relative orientation can be performed to determine the overlap and rotation angle between the images of the stereopair. Mismatches should be detected and removed while calculating relative orientation parameters.

Typical results of matched conjugate points of two stereopairs using the SIFT operator are shown in Figs. 11 and 12, respectively. As can be seen, there are large roll and yaw angles, respectively. However, most conjugate points matched by the improved SIFT operator are correct. The precision of these points matched by the SIFT operator is about 1 pixel. This is more than adequate to determine the overlap and rotation angle between an image pair although there are still a few mismatches.

FIG. 11. Matched conjugate points by SIFT operator of a stereopair with 15-degree roll angle.

FIG. 12. Matched conjugate points by SIFT operator of a stereopair with 8-degree roll and 22-degree yaw angle.

Feature Point Extraction. Extraction of feature points from images is the objective of all area-based image matching algorithms. There are many well-known feature point extraction operators, such as Moravec, Förstner, Harris and so on (Moravec, 1977; Förstner and Gülch, 1987; Harris and Stephens, 1988). Usually, the Harris detector can detect more apparent features, while the Förstner operator can achieve sub-pixel precision of feature points. So feature points from all images are firstly extracted with the Harris detector and then refined to the sub-pixel level with the Förstner operator. In this process, each image is divided into regular grids with predefined grid size, for example, 90×90 pixels. One feature point with the strongest interest value is extracted from each grid. For the Kodak camera used in this study and with 90×90 pixels grid size, at most 1650 feature points can be extracted from each image.

Precise Matching with Least Squares Strategy. Fine matching can be performed as long as approximate overlap and rotation angles are available. A pyramid-based matching strategy, which is usually adopted by traditional image matching algorithms, is also used for fine matching. The overlap of a stereopair determined by SIFT operator can be used to predict the initial position of a possible conjugate point for a certain feature point. Then precise least squares image matching is used to find the conjugate point in a local searching range around the predicted position along the epipolar line. After more conjugate points are matched, relative orientation is again performed to refine the orientation parameters. Gross mismatches are detected and removed in the relative orientation process. Then precise matching is again performed. Usually, matched points will be stable within three iterations. Note that for convenience of linking all stereomodels automatically, matched image points in one stereopair should be transferred to the next stereopair. This can be realised by treating the matched conjugate point from the previous stereopair as the first feature point in the same grid of the next stereopair.

Relative Orientation and Model Link

Relative orientation can be used to determine the orientation parameters of the right image when those of the left image are taken as known. Orientation parameters of the first image are

usually assumed to be zero. At the same time, mismatches that do not obey the coplanarity condition can be detected and removed. As mentioned above, there are often large rotation angles between adjacent low-altitude images. Sometimes the relative orientation process diverges because of the ill-posed problem of solution of normal equations, especially when there are some outliers among the conjugate points. Advanced outlier detection techniques should be applied. Gross mismatches are detected with the random sample consensus (RANSAC) strategy, while subtle outliers are detected by a robust estimation strategy of relative orientation with all conjugate points treated as simultaneous observations. Note that most outliers between image pairs belonging to different strips can also be detected by relative orientation. There are usually significant lens distortions in images acquired by non-metric cameras. Pre-calibrated lens distortion parameters should be considered in the relative orientation process.

All models in one strip can be automatically linked together by determining the baseline length with pass points derived from the image matching process. Note that if there are apparent rotation angles between two models, only calculating the correction of baseline length is not enough to link the two models. In this case, linking two models by calculating the similarity transformation parameters with two sets of model points is more reasonable. If a set of images includes two or more strips, orientation parameters should be transformed through common points between adjacent strips (except for the first strip). This can also be done by calculating the seven rigid transformation parameters between two strips with coordinates of common points.

Bundle Adjustment

There are inevitably discrepancies among camera parameters and model coordinates of conjugate points after linking successive models. So a free network bundle adjustment of the whole block, taking the orientation parameters of the first image and the baseline length of the first pair as known, is performed to eliminate these discrepancies and thus obtain stable internal geometric convergence. Then absolute orientation parameters (usually seven in number) can be easily calculated from the model coordinates and the real-world coordinates of GCPs.

Bundle adjustment with GCPs is the key to the analysis of geometric accuracy and a prerequisite for 3D information extraction. The collinearity equation is still the basic mathematic model of bundle adjustment. Because the camera used for data acquisition is usually non-metric, interior orientation parameters will change a little from time to time. The pre-calibrated interior and lens distortion parameters will not be exactly the same as the true values at the time of data acquisition. So a self-calibration strategy is expected to be used in bundle adjustment. Furthermore, as in traditional film-based photogrammetry, there is also apparent systematic error in coordinates of images acquired by digital cameras (Cramer, 2007). In this paper, correction polynomials of the 44-parameter Grün model are used in the bundle adjustment. The self-calibration parameters are closely correlated with the additional systematic parameters. So the two sets of parameters should never be treated as the unknowns of bundle adjustment at the same time.

A great advantage of low-altitude images is that the endlap and sidelap are both greater than in traditional photogrammetry, and thus any ground point usually has several corresponding image points. Another advantage is that the accuracy and reliability of bundle adjustment of low-altitude images will also be better since there are more redundant observations. So the accuracy achieved by bundle adjustment should be superior to that of traditional photogrammetry.

Textured 3D Building Model Generation

Three-dimensional building models with fine textures are key aspects of 3D city landscapes (Zhang et al., 2005). In this paper, building models are interactively generated by stereoscopic data capture using a digital photogrammetric workstation. When all buildings of interest have been captured by a human operator, they can be back-projected onto the image to retrieve corresponding textures of building roofs and walls. The texture of a building roof is usually taken from the middle image among all the target images in which it is visible. As for the texture of a wall which appears in multiple images, the image with maximum projected area is selected to provide the texture. Note that there are usually many textures occluded by tall trees or buildings, which can be semi-automatically refined under the control and supervision of the operator to generate realistic 3D city models (Zhang et al., 2005). Finally, the reconstructed building models are superimposed on the corresponding DOM and realistically visualised.

EXPERIMENTS AND RESULTS

Low-altitude images and GCPs are used as sources of information for experiments on the proposed approaches. Results of image matching and bundle adjustment, and digital photogrammetric products such as DSMs, DOMs and 3D building models, will be discussed in the following.

Image Matching

The proposed image matching approach generates about 600 to 800 successfully matched conjugate points in each image pair. Fig. 13 shows the matched conjugate points of one stereopair. As can be seen, all conjugate points are randomly distributed in the overlap areas. These conjugate points are enough for bundle adjustment. They can also be used to analyse the endlap and sidelap or relative rotation angles between adjacent images. The mean endlap between adjacent images fitted well with the predefined 80% value. The maximum endlap

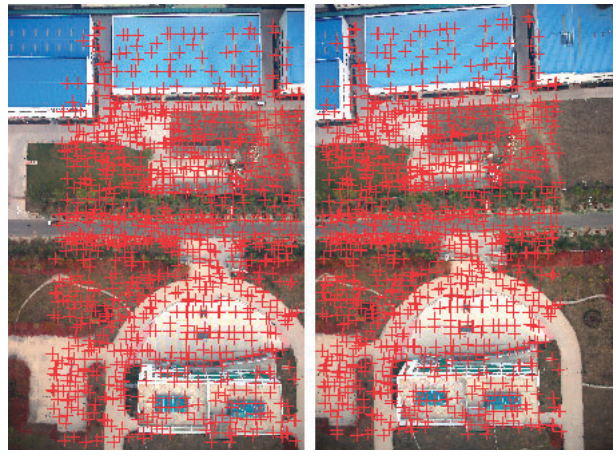

FIG. 13. Matched conjugate points of a stereopair.

FIG. 14. Matched conjugate points of images of adjacent strips.

between adjacent image pairs is about 85%, and the minimum is about 75%. The maximum sidelap between images of adjacent strips is about 80%, and the minimum is about 70%. As compared with the predefined 80% endlap and 75% sidelap, maximum overlap variation is about 5% in both directions.

The maximum relative rotation angle between adjacent images of the same strip is usually less than 5 degrees. However, rotation angles between images of different strips are usually larger than those along the same strip. As shown in Fig. 14, the yaw (κ) between two images of adjacent strips is about 12 degrees. In some extreme cases, the relative rotation angle of images belonging to adjacent strips is nearly 20 degrees. As can be seen in Fig. 14, most of the matched conjugate points are correct ones, which shows that the proposed algorithm is powerful for low-altitude image matching. These conjugate points of adjacent-strip stereoscopy are vital for aerial triangulation because they can link different strips together.

Bundle Block Adjustment

The accuracy of terrestrial feature extraction is one of the key problems faced by the low-altitude photogrammetric system. It directly determines whether the system can be used in practice. To fully evaluate the accuracy that the low-altitude images can achieve, bundle adjustment experiments with GCPs are performed. Previous experiences of bundle adjustment show that lens distortion parameters taken as unknowns are not as effective as additional parameters to model the systematic error of image coordinates. Only additional parameters are used to model the systematic error of image points in the following experiments.

Adjustment with 80% Endlap and 75% Sidelap Image Data of the North Testfield. Image data covering all 13 strips is used as the source of information. A total of 28 469 ground points were obtained by image matching. Each of them has at least three corresponding image points. The maximum number of corresponding image points of one ground point is 27, which is impossible in traditional photogrammetry. As shown in Fig. 5, 33 of the 64 ground points are used as GCPs, and the other 31 are check points in the bundle adjustment. The bundle adjustments using image data from 13 strips include two experiments, the first with additional

TABLE I. Accuracy of bundle adjustment with additional parameters using 80% endlap and 75% sidelap data (m).

		Rms	*Mean*	*Maximum*
Control points	*X*	0·015	0·003	0·043
	Y	0·013	−0·001	−0·030
	Z	0·018	0·002	−0·052
Check points	*X*	0·011	−0·002	0·025
	Y	0·010	−0·004	−0·028
	Z	0·021	−0·004	−0·061

parameters as unknowns and the second without. All configurations of bundle adjustment are exactly the same for the two experiments.

Unit weight root mean square (rms) error of the first experiment is 0·0023 mm, or better than 0·3 pixels. Error statistics of GCPs and check points are shown in Table I. As can be seen, the rms error of planimetric position and height of GCPs are both better than 0·02 m. The rms error of planimetric position of check points is also quite small, and the rms error of height is a little larger than 0·02 m, at about 0·4 GSD. The maximum errors of GCPs and check points are all smaller than 3 times the corresponding rms error, which means that there is no outlier among the control and check points. Because only 60% endlap and 30% sidelap is used by traditional photogrammetry, the height accuracy is usually around 1·0 to 1·5 GSD. So the achieved height accuracy of check points against the GSD in this experiment is definitely superior to that of the traditional photogrammetric process.

The results of bundle adjustment without additional parameters are shown in Table II. Unit weight rms error is also 0·0023 mm. As can be seen, the accuracy of planimetric position of GCPs and check points is similar to the first experiment, while the height accuracy is distinctly decreased. For example, the height accuracy of check points is about 1·3 GSD, more than 3 times the value achieved in the first experiment. The maximum error of check points is also 3 times that of the first experiment. This result shows that additional parameters are essential in bundle adjustment with image data acquired by a non-metric digital camera, even when it has been calibrated in advance.

Adjustment with 80% Endlap and 50% Sidelap Image Data of the North Testfield. To evaluate the relationship between height accuracy and sidelap, image data from alternate strips (7 strips out of the 13) was used as input data for bundle adjustment. There are a total of 17 596 ground points in this test data-set. Each ground point has at least three corresponding image points. The maximum number of corresponding image points of one ground point is 14. GCPs and check points are the same as in the experiment above. The bundle adjustment with seven

TABLE II. Accuracy of bundle adjustment without additional parameters using 80% endlap and 75% sidelap data (m).

		Rms	*Mean*	*Maximum*
Control points	*X*	0·019	−0·003	−0·060
	Y	0·018	−0·006	−0·090
	Z	0·039	−0·012	−0·083
Check points	*X*	0·008	−0·002	−0·018
	Y	0·014	−0·006	−0·051
	Z	0·065	0·026	0·186

strips also includes two experiments, the first with additional parameters and the second without. All configuration parameters of bundle adjustment are exactly the same as those in the above section.

Unit weight rms error of bundle adjustment with additional parameters is 0·0024 mm. Error statistics of control and check points are shown in Table III. As can be seen, rms errors of planimetric position of GCPs and check points are both better than 0·02 m. Rms errors of height of GCPs and check points are about 0·03 m, or 0·6 GSD. When compared with the result of the above section, the height accuracy is apparently decreased.

The results of bundle adjustment without additional parameters are shown in Table IV. Unit weight rms error is again 0·0024 mm. As can be seen, accuracy of planimetric position of GCPs and check points has decreased a little, while height accuracy is distinctly decreased. For example, the height accuracy of check points is about 1·6 GSD, nearly 3 times the accuracy with additional parameters. This result also verifies that additional parameters are essential in bundle adjustment.

As can be seen from the experimental results of bundle adjustment, when compared with the 0·05 m GSD, height accuracy of about 0·4 and 0·6 GSD can be achieved with low-altitude non-metric image sequences and 75 and 50% sidelap, respectively. Bundle adjustment with additional parameters can significantly improve the height accuracy. The achieved height accuracy is significantly higher than the traditional aerial triangulation.

Adjustment with 80% Endlap and 60% Sidelap Image Data of the South Testfield. Image data for all the 26 strips of the South testfield was used as the source of information for bundle adjustment. A total of 112 668 ground points were obtained by image matching. Each of these ground points has at least three corresponding image points. The maximum number of image points corresponding to one ground point is 24. As shown in Fig. 8, 130 of the 190 ground

TABLE III. Accuracy of bundle adjustment with additional parameters using 80% endlap and 50% sidelap data (m).

		Rms	*Mean*	*Maximum*
Control points	*X*	0·016	0·003	0·042
	Y	0·012	−0·001	0·033
	Z	0·029	0·004	−0·087
Check points	*X*	0·016	0·004	0·029
	Y	0·011	−0·002	−0·027
	Z	0·027	0·001	−0·070

TABLE IV. Accuracy of bundle adjustment without additional parameters using 80% endlap and 50% sidelap data (m).

		Rms	*Mean*	*Maximum*
Control points	*X*	0·017	−0·001	0·058
	Y	0·020	−0·001	−0·067
	Z	0·068	−0·013	−0·235
Check points	*X*	0·027	−0·006	−0·081
	Y	0·021	−0·011	−0·076
	Z	0·080	−0·014	−0·277

TABLE V. Accuracy of bundle adjustment with additional parameters using 80% endlap and 60% sidelap data (m).

		Rms	*Mean*	*Maximum*
Control points	*X*	0·116	0·005	0·266
	Y	0·118	−0·002	0·281
	Z	0·129	0·005	0·369
Check points	*X*	0·130	0·014	−0·242
	Y	0·124	0·003	0·295
	Z	0·167	0·017	0·444

points were used as GCPs, and the other 60 are check points in the bundle adjustment. Bundle adjustment with additional parameters was performed for this data-set.

Unit weight rms error of the experiment is 0·0033 mm, or about 0·4 pixels. Error statistics of GCPs and check points are shown in Table V. As can be seen, the rms errors of planimetric position and height of GCPs are better than 0·17 and 0·13 m, respectively, while the rms errors of planimetric position and height of check points are both better than 0·2 m. The maximum errors of GCPs and check points are all smaller than 3 times the corresponding rms error.

Digital Photogrammetric Products

Once aerial triangulation is finished, a DSM can be generated by dense image matching and forward intersection. Firstly, feature points are extracted with a dense grid of every 11×11 pixels in each image. Then conjugate points are found by the multi-image matching algorithm under the constraints of already matched conjugate points for bundle adjustment and the known camera parameters. Finally, corresponding ground coordinates of all the matched conjugate points are calculated by multi-image forward intersection. These ground points can be used to generate Delaunay triangles, which form the common data structure to represent 3D terrain information.

A DOM can be generated by orthorectification from low-altitude images with known camera parameters and the DSM already obtained. Mosaic lines abutting adjacent ortho-images should not pass through objects above the ground, such as buildings and trees. The colour and illumination of images acquired by digital cameras, especially images belonging to different strips, are usually different. So the ortho-image thus generated has to be further processed by image dodging or other colour adjustment techniques. The resulting ortho-images of the North and South testfields after colour adjustment are shown in Figs. 15 and 16, respectively. The accuracy of a DOM can be checked by using known ground features such as GCPs. Coordinates of GCPs can be interactively measured from an ortho-image and then compared with the ground coordinates from the field survey. Accuracy of the ortho-images was about 0·045 and 0·20 m, respectively, for the two data-sets when measured coordinates of GCPs were compared with their field survey coordinates. Coordinates of all GCPs are also measured by stereomodel and compared with the known coordinates. Both planimetric and height accuracy of the first test data-set are better than 0·05 m, which means that the proposed approach and the images acquired by the low-altitude photogrammetric system meet the national mapping criterion for 1:500 scale mapping with its maximum limits of 0·15 m in planimetry and 0·10 m in height.

DEM and DOM products were successfully generated from the data, within one and three days for the North and South data-sets, respectively, using the parallel processing strategy. The

FIG. 15. Digital ortho-image of the North testfield.

FIG. 16. Digital ortho-image of the South testfield.

traditional approach with a single computer takes at least 3 and 10 days, respectively. That means the efficiency of parallel processing is at least 3 times that of the traditional approach.

The 3D city model is one of the most important photogrammetric products. It is very useful for city planning, car navigation, online shopping and so on. Low-altitude images

FIG. 17. 3D visualisation of building models of the North testfield.

FIG. 18. 3D visualisation of building models of the South testfield.

processed as described in this paper are advantageous in generating 3D building models and fine textures because of their characteristics of high endlap and sidelap. Up to now, automatic reconstruction of 3D building models has been very difficult. Semi-automatic 3D model construction with VirtuoZo software was adopted for the work described in this paper. Textures of building models are automatically obtained by the proposed approach. 3D visualisations of several textured buildings of the two testfields are shown in Figs. 17 and 18. As can be seen, the textured building models are very realistic. They have considerable potential in various applications that need 3D visual models.

CONCLUSIONS

The principles and technologies of photogrammetric processing of low-altitude images acquired by unpiloted aerial platforms are discussed in this paper. The major advantage of low-altitude UAVs is that images can be acquired under cloud with very high ground resolution. This methodology is very promising for applications requiring a quick response, such as

disaster monitoring. Furthermore, the geometric configuration of low-altitude image sequences is also stronger with stereoscopy resulting from large endlaps and sidelaps. The accuracy and reliability of bundle adjustment are also higher since there are more redundant observations.

The proposed image matching approach can automatically find conjugate points from image pairs with different overlaps and large rotation angles. High-order correction polynomials used in bundle adjustment can significantly improve the height accuracy. First results of image matching and bundle adjustment are very satisfactory. Under the experimental conditions of low-altitude images with 80% endlap and 50% sidelap, 0·05 m GSD and 0·40 base-to-height ratio, the accuracy of the products generated meets the Chinese national criteria for 1:500 scale mapping. The experimental results show that the proposed approaches and the low-altitude photogrammetric system developed here are promising for large scale digital photogrammetry and precise 3D reconstruction.

Integration of a differential GPS receiver into the low-altitude platform to measure precise coordinates of each exposure station and thus decrease the number of required GCPs is the important work to be performed in the near future.

Acknowledgements

This work was supported by National Natural Science Foundation of China with project number 41071233, National Key Technology Research and Development Program with project number 2011BAH12B05, National Hi-Tech Research and Development Program with project number 2009AA121403 and Program for New Century Excellent Talents in University with project number NCET-07-0645. The authors also acknowledge the assistance of the Editorial team of *The Photogrammetric Record* including the helpful guidance provided by Newby (2007).

References

Altan, M. O., Celikoyan, T. M., Kemper, G. and Toz, G., 2004. Balloon photogrammetry for cultural heritage. *International Archives of the Photogrammetry, Remote Sensing and Spatial Information Sciences*, 35(B5): 964–968.

Bitelli, G., Girelli, V. A., Tini, M. A. and Vittuari, L., 2004. Low-height aerial imagery and digital photogrammetrical processing for archaeological mapping. *International Archives of the Photogrammetry, Remote Sensing and Spatial Information Sciences*, 35(B5): 498–503.

Coppa, U., Guarnieri, A., Camarda, M. and Vettore, A., 2010. Development of unmanned aerial vehicle at Padova University. *International Archives of the Photogrammetry, Remote Sensing and Spatial Information Sciences*, 38(5): 173–177.

Cramer, M., 2007. The EuroSDR performance test for digital aerial camera systems. *Photogrammetric Week 2007*, Wichmann, Heidelberg. 89–106.

Förstner, W. and Gülch, E., 1987. A fast operator for detection and precise location of distinct points, corners and centres of circular features. *Proceedings of ISPRS Intercommission Conference on Fast Processing of Photogrammetric Data*, Interlaken, Switzerland. 437 pages: 281–305.

Harris, C. and Stephens, M., 1988. A combined corner and edge detector. *Proceedings of Fourth Alvey Vision Conference*. 147–151.

Huang, H.-H. and Lin, S.-Y., 2003. Digital photogrammetry using tethered balloon. *Journal of Photogrammetry and Remote Sensing of Taiwan*, 8(2): 55–68.

Karras, G. E., Mavromati, D., Madani, M., Mavrelis, G., Lymperopoulos, E., Kambourakis, A. and Gesafidis, S., 1999. Digital orthophotography in archaeology with low-altitude non-metric images. *International Archives of Photogrammetry and Remote Sensing*, 32(5/W11): 8–11.

Lin, Z. J., 2008. UAV for mapping—low altitude photogrammetric survey. *International Archives of the Photogrammetry, Remote Sensing and Spatial Information Sciences*, 37(B1): 1183–1186.

Lowe, D. G., 1999. Object recognition from local scale-invariant features. *Proceedings of 7th IEEE International Conference on Computer Vision*, 2: 1150–1157.

LOWE, D. G., 2004. Distinctive image features from scale-invariant keypoints. *International Journal of Computer Vision*, 60(2): 91–110.

MORAVEC, H. P., 1977. Towards automatic visual obstacle avoidance. *Proceedings of the 5th International Joint Conference on Artificial Intelligence*, 2: 584–585.

NAGAI, M., CHEN, T. E., AHMED, A. and SHIBASAKI, R., 2008. UAV borne mapping by multi sensor integration. *International Archives of the Photogrammetry, Remote Sensing and Spatial Information Sciences*, 37(B1): 1215–1222.

NEWBY, P. R. T., 2007. Technical terminology for the photogrammetric community. *Photogrammetric Record*, 22(118): 164–179.

NOGAMI, J., PHUON, D. M. and KUSANAGI, M., 2002. Field observation using flying platforms for remote sensing education. *23rd Asian Conference of Remote Sensing*, Kathmandu, Nepal, Paper ID: ED02-2 (on CD-ROM).

ZHANG, Y., 2008. Photogrammetric processing of low altitude image sequences by unmanned airship. *International Archives of the Photogrammetry, Remote Sensing and Spatial Information Sciences*, 37(B5): 751–758.

ZHANG, Y., ZHANG, Z., ZHANG, J. and WU, J., 2005. 3D building modelling with digital map, lidar data and video image sequences. *Photogrammetric Record*, 20(111): 285–302.

ZHANG, Z., ZHANG, Y., KE, T. and GUO, D., 2009. Photogrammetry for first response in Wenchuan earthquake. *Photogrammetric Engineering & Remote Sensing*, 75(5): 510–513.

Résumé

Les images acquises à basse altitude par des véhicules aériens sans pilote présentent plusieurs avantages: un recouvrement important, des angles de visée multiples et une très haute résolution au sol. De telles images peuvent être utilisées pour différentes applications nécessitant une grande précision ou une texture fine. Une nouvelle approche est proposée pour le traitement parallèle d'images acquises à basse altitude par des véhicules aériens sans pilote, capables de voler en mode automatique selon des lignes de vol prédéfinies, sous le contrôle d'un système autopiloté. Le taux moyen de recouvrement et les angles de rotation relative entre images adjacentes sont estimés par une corrélation globale basée sur un opérateur SIFT amélioré. Des points conjugués et les paramètres d'orientation relative sont déterminés avec précision grâce à une stratégie pyramidale d'appariement d'images par moindres carrés et au processus d'orientation relative. La compensation par faisceaux est réalisée au moyen de points de liaison appariés automatiquement et de points d'appui mesurés de manière interactive. Après l'aérotriangulation, les images à haute résolution peuvent être utilisées avantageusement pour obtenir des données spatialisées précises comme des modèles numériques de surface (MNS), des orthophotoplans numériques et des modèles urbains 3D. Une stratégie de traitement parallèle est introduite pour améliorer la rapidité du processus photogrammétrique. Des résultats expérimentaux montrent que l'approche proposée convient au traitement d'images acquises à basse altitude et présente un potentiel élevé pour l'acquisition d'informations spatiales à grande échelle et la modélisation précise en trois dimensions.

Zusammenfassung

Luftbilder, die von unbemannten Flugobjekten aus geringer Höhe aufgenommen werden, bieten hohe Überlappungsraten, mehrfache Ansichten eines Objektes und eine sehr hohe Bodenauflösung. Für die verschiedensten Anwendungen, die eine hohe Genauigkeit oder die Erfassung feiner Texturen erfordern, können diese Luftbilder verwendet werden. Zur Auswertung der Aufnahmen der unbemannten Flugzeuge wird ein Vorschlag zur Parallelprozessierung präsentiert. Die unbemannten Flugobjekte

fliegen vordefinierte Flugrouten mit Hilfe eines Autopiloten ab. Die Überlappung und die relativen Orientierungswinkel zweier aufeinanderfolgender Aufnahmen werden durch Bildzuordnung auf der Basis eines verbesserten Scale Invariant Feature Transform (SIFT) Operators bestimmt. Eine Kleinste Quadrate Zuordnung und eine relative Orientierung dienen zur Bestimmung homologer Punkte und der relativen Orientierungswinkel. Die Bündelausgleichung stützt sich auf automatisch zugeordnete homologe Punkte und manuell gemessene Passpunkte. Die Ergebnisse dieser Aerotriangulation dienen als Grundlage für die Ableitung digitaler Oberflächenmodelle, digitaler Orthophotokarten und 3D Stadtmodellen. Durch die parallele Prozessierung soll die Effizienz des photogrammetrischen Prozesses gesteigert werden. Die experimentellen Untersuchungen bestätigen, dass die vorgeschlagenen Ansätze in der Lage sind, derartige Aufnahmen zu prozessieren und generell ein großes Potential besitzen, Rauminformation für großmaßstäbige Karten schnell und genau dreidimensional zu erfassen.

Resumen

Las imágenes aéreas tomadas a baja altura por vehículos aéreos no tripulados ofrecen múltiples ventajas como el elevado solape, múltiples ángulos de toma y una resolución en el terreno muy alta. Este tipo de imágenes puede utilizarse en aquellas aplicaciones que exijan una elevada precisión o una textura fina. Se ha desarrollado un nuevo procedimiento para el procesado paralelo de imágenes tomadas por estos vehículos, que pueden volar automáticamente siguiendo rutas predefinidas controlados por un sistema de navegación automático. Los ángulos de solape global y de rotación relativa entre dos imágenes adyacentes se estiman por correspondencia global con un operador SIFT mejorado. Los puntos homólogos y los parámetros de orientación relativa se determinan con precisión mediante una estrategia de correspondencia de imágenes basada en una pirámide de mínimos cuadrados y el proceso de orientación relativa. El ajuste por haces se basa en puntos homólogos obtenidos automáticamente y en puntos de apoyo terrestre medidos interactivamente. Tras este proceso de triangulación aérea las imágenes de alta resolución pueden utilizarse para la obtención de productos cartográficos precisos tales como modelos digitales de superficie, ortofotomapas digitales y modelos urbanos tridimensionales. Se presenta una estrategia de proceso paralelo con el objetivo de mejorar la eficiencia del proceso fotogramétrico. Los resultados experimentales indican que los métodos propuestos son efectivos para procesar imágenes tomadas a baja altura, lo que permite mejorar la obtención de información espacial a escalas grandes, una rápida respuesta y un modelado tridimensional preciso.